Object extraction from Remote Sensing images and Image / Elevation data aggregation for Realistic 3D Rendering.

C. Maire, M. Datcu
Remote Sensing Technology Institute (IMF).
German Aerospace Center (DLR) D-81234 Weßling, Germany
{cyrille.maire, mihai.datcu}@dlr.de

Keywords: InSAR DEM filtering, segmentation, topology, object modeling, fusion, regularization

ABSTRACT: We present a complete processing line to enhance large Remote Sensing (RS) image databases in the framework of real-time 3D rendering. RS and Virtual Reality communities are faced to several challenges to deal in real-time with large image datasets while preserving high quality and realistic rendering. There is an increasing interest of InSAR (Interferometric Synthetic Aperture Radar) data, due to principally with the availability of a near global coverage of HR DEM with the Shuttle Radar Topography Mission (SRTM). Important improvements of DEM are needed to provide more realistic visualizations. DEM pre-processing are performed by exploiting only the couple of data required for 3D visualization. A non stationary bayesian filter is presented to remove noise and small artifacts which pervade the InSAR DEM while preserving structural information. To produce more realistic rendering, information from optical images are fused in the DEM data. An object based description of large optical Remote Sensing (RS) images is obtained in two stages. (i) The optical image is segmented to simplify the amount of data. (ii) A novel dynamical algorithm is proposed to extract the regions and geometry which are stored in a tree structure that defines spatial relationships between regions (e.g. adjacencies, inclusions). An interactive object selection procedure links the extracted objects to their elevation modeling. The objects 3D structure is estimated from the DEM data using its planimetric shape extracted from the optical image and the elevation modeling assigned. The proposed object line processing provides more realistic 3D visualizations.

1 INTRODUCTION

Land cover mapping is realized using the synergy between RS data types: DEM provides a basic spatial reference system and image data can be draped over the DEM for more advanced analyses. Up to now, the exploitation of large and complex RS databases in the overall interactive 3D visualization process is extremely difficult. The demand for such technologies leads to a reinforcement of world acquisition programs (SRTM, largest homogenous coverage acquisition) and tools to fully exploit such datasets. In [1] an efficient real-time rendering algorithm is proposed. In addition to the rendering time constraints, realistic visualizations require significant DEM enhancement and regularization since it brings the geometry information.

In order to generate more realistic 3D rendering of RS data, several methods to enhance DEM are proposed (Fig. 1) [2]. Based on DEM data, a filtering (i) is applied. To gather complementary information for DEM regularization, an object based description of large optical images is developed (Fig. 2). It consists of two sequential and independent stages; (ii) segmenting large images; (iii) generating dynamically an object-oriented image description that reflects both geometry of the extracted objects and their topological relations (adjacencies, inclusions). A merging algorithm (iv) is proposed to fuse image-object in the DEM data.

To filter DEM (i), the efficiency of classical methods [3], [4] generally used for SAR despeckling is limited by an incomplete noise modeling. Multi-resolution filtering approaches [5], [6] lead to poor realistic visualization due to the generation of shrinkage artifacts traduced by unnatural aspects [7]. In [8], [9], a Bayesian filter has been developed to deal with non-stationary data such as InSAR DEM. By using Gauss Markov Random Fields (GMRF) models it attempts to remove thermal and coherent noises while preserving structural information.

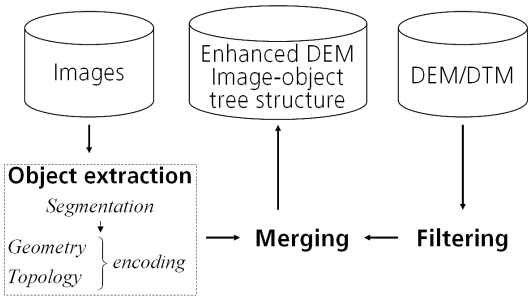

Fig. 1: System flowchart.

Segmentation processes (ii) aim to subdivide the image into disjoint regions characterized by similar properties. In [10], a wide review of image segmentation techniques is presented. Region-based methods exploit directly spatial information in order to group homogenous pixels into closed and connected regions. Both methods; Bayesian [11], MeanShift [12], region growing [13], Minimum Description Length [14] or Morphological are providing satisfactory results for a given purpose. In order to deal with regions expressed as objects, their respective geometry and topological properties need to be extracted.

To achieve topology descriptions, various discrete spatial models are proposed [15], [16]. The complex cellular approach [15] is particularly well suited since it turns out the connectivity paradox and topological problems with Z^2 (i.e. with discrete grid). The plane (R^2) is decomposed in regular complex cells, which replace the pixel model (Z^2). A discrete model is generated that preserves the topology of R^2 in a similar way as manipulating vectors models. Based on this modeling, geometry and adjacency relations of the regions can be expressed. We propose to complete the object representation by investigating the inclusion relationships between regions [17]. A tree structure is presented to store the regions and reflects their topological properties.

In [18], [19], DEM regularization approaches (iv) have been proposed. Landscape cover types are extracted from existing Geographic Information System (GIS) databases and formulated as elevation constraints. In this paper, only the visualization dataset (optical image and DEM) is used; Regions are extracted from the optical image (texture) and linked to their thematic representation by an interactive object selection procedure (i.e. to include human knowledge in the system). The selected information in form of objects is merged with the filtered DEM by assigning elevation constraints. A Least Square Problem is formulated to optimize the adjustment and completed by morphologic operations.

This paper is organized as follows. In section 2, an InSAR DEM filter is presented. A segmentation algorithm for optical images is presented in section 3. Section 4 describes the structure of the dynamical object database. A DEM regularization process is proposed and illustrated by examples in section 5.

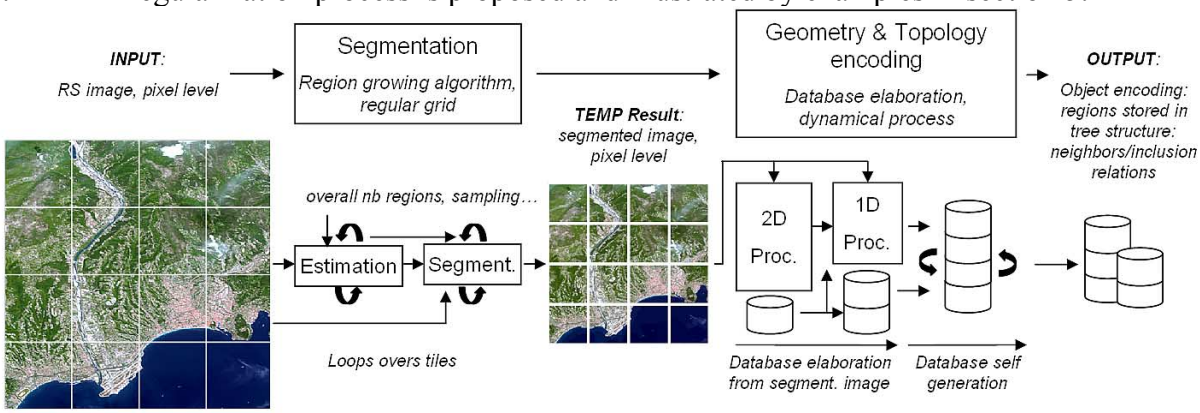

Fig. 2: Flowchart of the object/region extraction algorithm: Starting from large RS image (pixel-oriented), two independent processes are designed to achieve an object oriented description of the image.

2 INSAR DEM FILTERING

The formerly most used method to produce elevation data consists in the interpolation of topographic digitized level curves [20]. The resulting information obtained (Digital Terrain Model) is characterized by smooth aspect, interpolation artifacts and differs from RS DEM. It contains only the terrain elevation information, while vegetative, urban elevations are not included. Indeed, for 3D visualization, such data are not efficient enough to reach the level of realism required by users. References [21], [22] give further details related on RS elevation data.

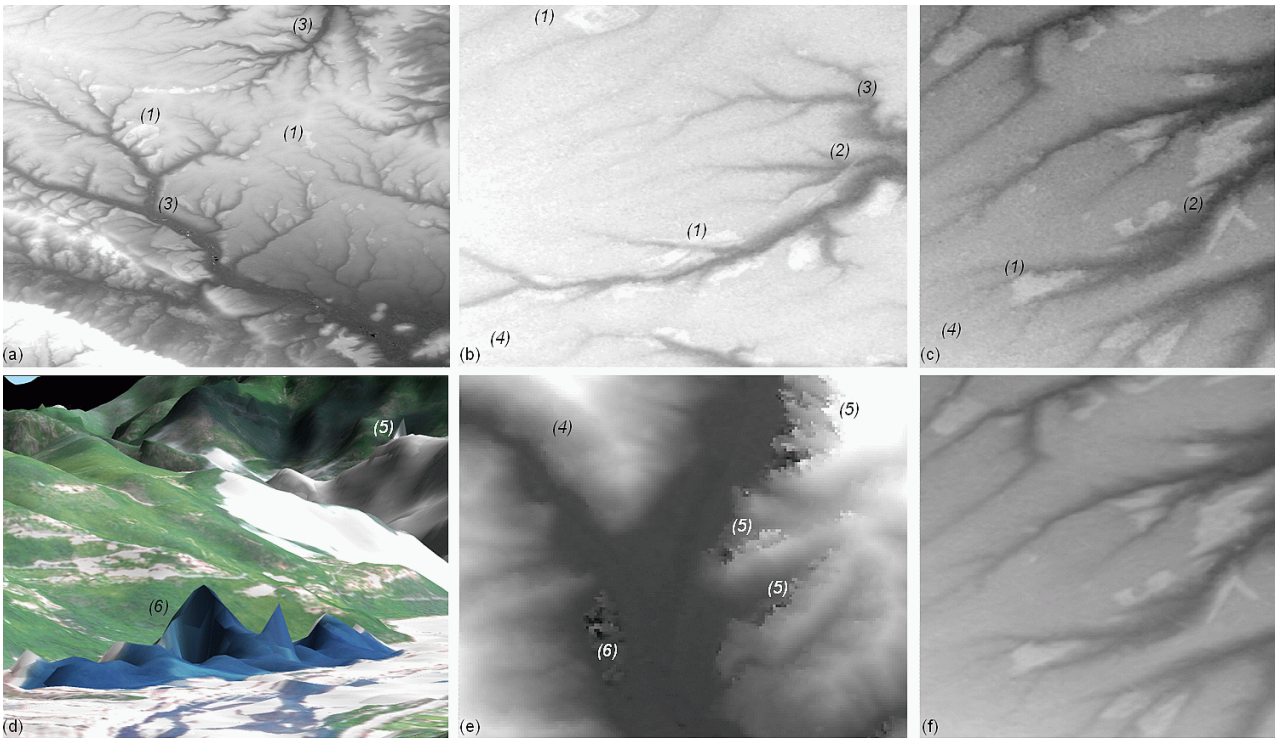

Fig. 3: InSAR X-SRTM DEM characteristics on smooth (a-c, f) and mountain (d, e) areas. Information content: Forest (1), valleys (2), large buildings, bridges. Noise and artifacts: Thermal and coherent noise (4), Phase Unwrapping artifacts (5), specular reflection on the lake surface (6). DEM filtering: (c) input raw data, (f) corresponding filtered DEM.

Fig. 3 presents the X-SRTM DEM data, generated by using an X-band single pass sensor on board of the Space Shuttle. InSAR DEMs contain, according to the acquisition process (resolution, sensor frequencies), at least partially some objects; "forest", "buildings", "sea", etc. Geometric displacements, artifacts, shadowed areas and inversions can occur depending on the acquisition conditions and the relief [23]. Both are characterized by an excessive roughness (too high fractal dimension / local variance). An essential issue is to remove the noises (thermal and low coherence) which pervade InSAR DEM. Land-covers have a direct influence (specular reflections on flat surfaces such as lakes, Fig. 3d-e).

A Bayesian filter has been developed to deal with non-stationary data such as InSAR DEM [8], [9]. It attempts to remove noise (assumption of uncorrelated and additive noise) from the InSAR DEM data while preserving structural information. Assuming the noise and SAR model formation, the process of filtering is considered as an ill-posed inverse problem, and formulated in the general frame of Bayesian inference in two levels:

- Model fitting: To filter the data, Maximum A Posteriori (MAP) method with a Gaussian distribution for the likelihood and GMRF models employed as prior.
- Model selection: Evidence Maximization computed for a library of models centered on a guess of the parameter to be estimated.

Given a noisy information y; estimates the most probable realization x, where θ is a vector parameter describing the neighborhood pixel relations. To filter the image y, a MAP estimation of the data is used choosing different prior models (maximization of the numerator in (1)). Indeed, in the first level of inference, the evidence is omitted (normalization term). To represent the prior model, which comes in the form of a texture model, GMRF models [8] are used (2) with x_η, the neighborhood system.

$$p(x \mid y,\theta) = \frac{p(y \mid x)p(x \mid \theta)}{p(y \mid \theta)} = \frac{likelihood \times prior}{evidence} \qquad (1)$$

$$p(x \mid x_\eta,\theta) = \frac{1}{\sqrt{2\pi\sigma^2}} exp\left(- \frac{(x - \sum_{j\in\eta} \theta_j x_j)^2}{2\sigma^2} \right) \qquad (2)$$

For analytical tractability, we use a library of models and perform a model selection (second level of inference) in order to get the model that best describes the data through the evidence calculation. Fig. 3f illustrates the non-stationary filtering performed on the raw SRTM DEM (Fig. 3c). The noise parameter estimation is efficient due to the complete and non-stationary noise modeling. The global aspect of the DEM is more realistic. A comparison with other well-known filters is presented in [7] and illustrates the efficiency of the presented DEM filter. Suitable results (in terms of statistical analyses and rendering aspects) are obtained, nevertheless large artifacts remained. In order to significantly enhance the DEM to produce more realistic flight simulations, complementary information have to be gathered from the optical image (Fig. 2).

Fig. 4: Image segmentation applied to SPOT5 "Supermode" color image, 2.5m resolution. {Respectively} Left: test site of {Nice, Toulouse} (France), tile of {1024, 512}-pixel square. Right: segmented image obtained for {1500, 1300} regions.

3 SEGMENTATION

A recursive region growing algorithm [13] is used to partition the image g into n disjoint regions R_i (3), where Ω is the image domain. The algorithm is based on the minimization of the simplest case Mumford and Shah functional and modeled by an energy functional $E(u, K)$ (4). u is the piecewise constant approximation of g and K denotes its dual, the boundary set. The boundary density ($|K|$ is the total length of K) is controlled by the scale parameter λ; the larger λ, the coarser the segmentation.

$$\bigcup_{i=1}^{n} R_i = \Omega \quad , \quad \forall \quad i \neq j \quad : \quad R_i \cap R_j = \varnothing \tag{3}$$

$$E(u, K) = \sum_{i=1}^{n} \sum_{R_i} \| u_{R_i} - g \|^2 + \lambda \mid K \mid \tag{4}$$

The algorithm is looking for a global energy reduction; the pair of adjacent regions $\{R_i, R_j\}$ which provides the biggest energy decrease (smallest merging cost λ_{ij} (5)) is merged and the shared boundary δR_{ij} is deleted. Starting from a regular grid of regions where each pixel is a region, the merging process is iteratively repeated until n regions remains. A finer-segmented result (n large) is preferred to a coarser one, since it is possible to refine the region merging after the topology analysis process.

$$E(K_{\setminus \delta R_{ij}}) - E(k) = \frac{\mid R_i \mid \times \mid R_j \mid}{\mid R_i \mid + \mid R_j \mid} \| u_{R_i} - u_{R_j} \|^2 - \lambda_{ij} \mid \delta R_{ij} \mid \tag{5}$$

As shown in Fig. 4, results obtained are promising. Some drawbacks remain: the algorithm depends on the intensity scale (quadratic term that controls the region homogeneity (4)) and the memory requirements are extremely important due to the regular grid initialization. To handle large datasets segmentation, the input image is tiled and a two-pass segmentation process is applied (Fig. 2). To distribute efficiently n regions among all the tiles, a complete segmentation is done to extract the evolution curve $f_{tile\ i}(\lambda) = n_{tile\ i}$ for every tile i. λ is estimated among all the segmentation evolution curves to get the best region density $n_{tile\ i}$ regarding the overall number of regions n. Assuming an estimated number of regions $n_{tile\ i}$ for each tile, a second pass segmentation is applied. The process is completed by the topology algorithm to handle border regularization between tiles.

4 GEOMETRY AND TOPOLOGY EXTRACTION

The segmentation algorithm generates a partition $\Omega_{w,h}$ of the image in disjoint regions (w, h denote the image size). Geometry and adjacency relations could be directly extracted during the segmentation process. A sequential approach presents the advantage to be independent from the segmentation method used. Using the complex cellular modeling [15], $\Omega_{w,h}$ is expressed by an inter-pixel representation $\Omega'_{w+1,h+1}$ composed of Nodes N (0-cells), Boundaries B (set of connected 1-cells). Using the set of nodes and boundaries extracted, Borders CB (closed set of connected boundaries) are constructed to represent the Regions R (2-cells). These definitions are illustrated in Fig. 5 and follows (6) - (15) with $(i, j, k, l) \in Z^4$. The resulting algorithm extracts and stores dynamically the various objects (0-1 cells) in a database D that contains both geometry and adjacency relations. The region modeling is achieved by collecting structural elements from D. A tree structure is designed to store the regions and reflects their topological properties.

4.1 *Topology: 4 connectivity neighborhood*

- Nodes $N \in Z^2$ ($\Omega'_{w+1,h+1}$). Using the inter-pixel representation, a node N (6) is the extremity of at least one boundary (closed boundary) or maximum four (Fig. 5b).

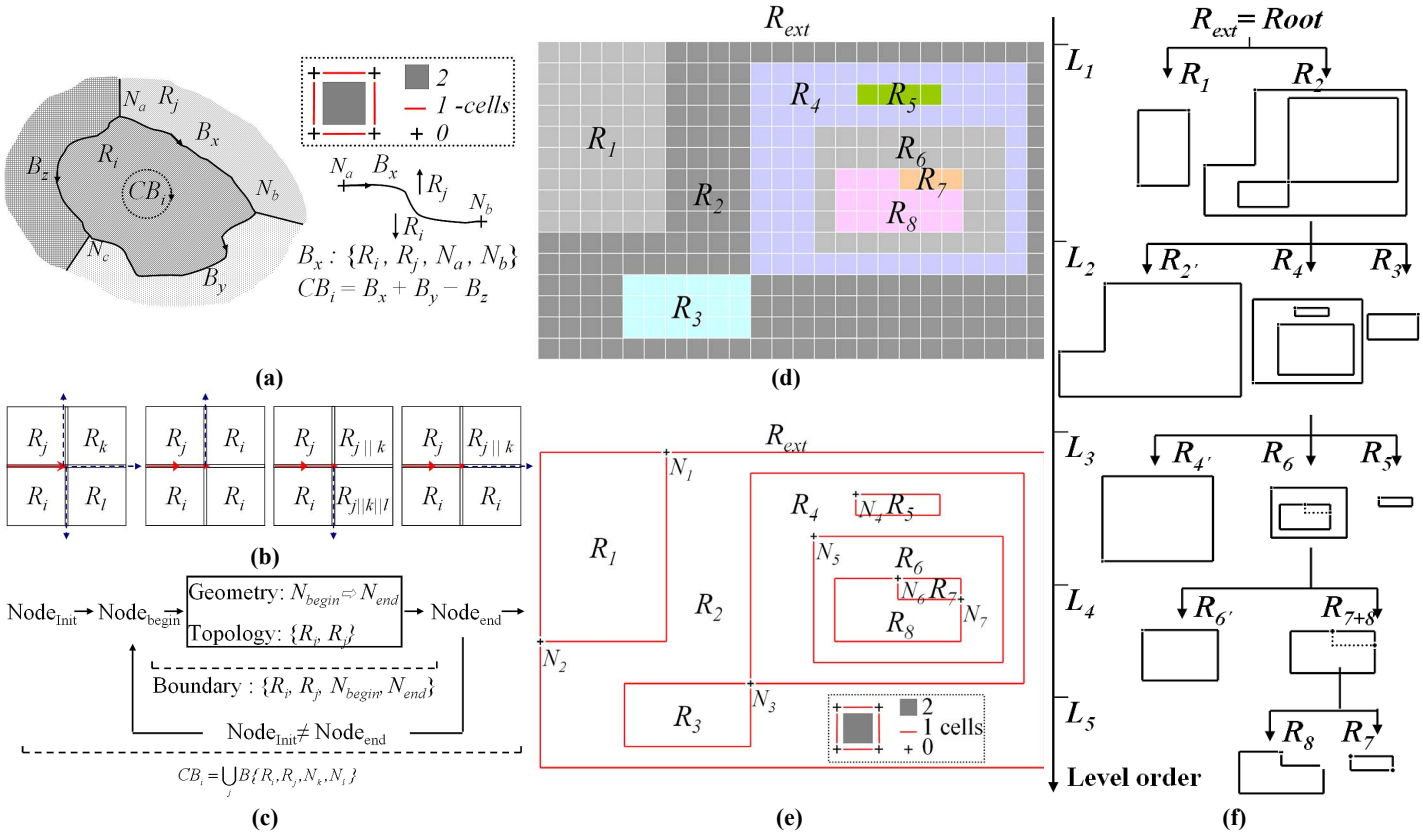

Fig. 5: Inter-pixel representation: (a) Object modeling. (b) Geometry: Freeman code (direction *T*, 1st left): For a given region R_i and an initial direction T_E, 3 direction cases. (c) Object generation process; Border CB_i (external border associated to the region R_i). Topology process: (d) Merging algorithm. (e) Shape extraction. (f) Tree structure.

- Boundary: B delimits two adjacent regions R_{right}, R_{left} and is oriented (9) (two nodes N_{begin}, N_{end}). The boundary shape from N_{begin} to N_{end} is described by a Freeman code (8) using k pairs $\{L, T\}$, where L denotes the number of 1-cells in a given tracking direction T (Fig. 5b). $|B|$ denotes the area underneath the boundary (7).

$$B_i \cap B_j = \begin{cases} \varnothing \\ \{N_k\} \| \{N_k, N_l\}, k \neq l \end{cases}, i \neq j \qquad (6) \qquad |B| = \frac{1}{2}\sum_{l=1}^{k}(y_{l+1}+y_l)L_l T_{l_x} \quad , \begin{cases} y_{l+1} = y_l + L_l T_{l_y} \\ \{y_1, y_{k+1}\} = \{y_{begin}, y_{end}\} \end{cases} \qquad (7)$$

$$N_{end} = N_{begin} + \sum_{l=1}^{k} L_l T_l \ , \ T_l(T_x, T_y) = \begin{cases} T_N(0,-1)\ T_E(1,0) \\ T_W(-1,0)\ T_S(0,1) \end{cases} \qquad (8) \qquad |B| + |B'| = 0 \ , \ B_{R_j,R_i,N_l,N_k} = -B'_{R_i,R_j,N_k,N_l} \qquad (9)$$

- Border: CB_i is a closed and oriented chain of connected boundaries: For each boundary B_j which belong to CB_i, a direction δ_j is associated (10) using (9). CB_i delimitates R_i from its external neighborhood regions (10)-(12) as shown in Fig. 5a. The interior region R_i' (11) is the entire area within CB_i. Since the chain is oriented in the clockwise turn, the area underneath the border $|CB_i|$ is strictly positive (13).

$$CB_i = \oplus_j \delta_j B_{R_i,R_j,N_k,N_l} \ with \ \delta_j = \begin{cases} 1 \ if \ R_j = R_{left} \\ -1 \ if \ R_j = R_{right} \end{cases} \qquad (10) \qquad R_i' \cap R_j' = R_j' \Leftrightarrow R_j \subset R_i \qquad (11)$$

$$CB_i \cap CB_j = \begin{cases} \{B\} \Leftrightarrow R_i \ and \ R_j \ are \ adjacent \\ \{N\} \| \varnothing \end{cases} \qquad (12) \qquad |CB_i| = \sum_j \delta_j |B_{R_i,R_j,N_k,N_l}|, |CB_i| > 0 \qquad (13)$$

- Region: A region R_i (1) is defined by one external border CB_i and a collection of internal disjointed borders $\{CB_j\}$ (14). Such modeling enables to investigate inclusion relationships between the regions. If a group of adjacent regions $\{R_a\}$ may constitute a "hole", a new border is created using the set of boundaries to represent the convex hull of $\{R_a\}$. It's corresponding region is a dummy region (Fig. 5f, R_{7+8}).

$$R_j \subset R_i, \ R_i = CB_i \oplus \bigcup_j CB_j \Leftrightarrow R_i = R_i' - \bigcup_j R_j' \qquad (14) \qquad \left.\begin{matrix} R_j \subset R_i \\ order_j = order_i + 1 \end{matrix}\right\} \Leftrightarrow \begin{cases} R_j \ is \ a \ child \ of \ R_i \\ R_i \ is \ the \ parent \ of \ R_j \end{cases} \qquad (15)$$

4.2 *Tree of regions*

A root tree structure is designed to store in a simple and "natural" way the regions according to their topology, but also to speed up data access. Nodes of the tree are regions and branches are reflecting the inclusion relationships between the regions. The root denotes the border of the processed image (Fig. 5f). It can be seen as an empty

region that covers the whole image where all the regions are included. In the tree construction, the "directed" notion is added. In a rooted directed tree, from a given region stored in the tree, there is only one path to the root. Given this directed notion of a rooted tree, a rooted sub-tree can be defined for each node of the tree. Hence, for each region which contains included regions, a sub-tree is recursively generated.
In the tree structure, the level order corresponds to the vertical distance from the root ($order_0$) (Fig. 5f). For a given sub-tree of the region Ri ($order_k$), the direct children ($order_{k+1}$) are siblings and have a unique parent R_i (15). In this case, R_i' is placed as first child of R_i as shown in Fig. 3d (regions R_2', R_4', R_6').The tree is directly reflecting the region relationships. For each region stored, we can directly access to the included/parent regions, (i.e. vertical navigation in the tree), or adjacent regions (horizontal navigation). Once the tree structure is stored, further complementary editing or modifications are possible in order to merge regions with spatial relationships.

4.3 *Algorithm flowchart*

The sequential process is described in three steps as shown in Fig. 5d-f:

- Step 1: A merging growing algorithm is performed in the segmented image $\Omega_{w,h}$, to retrieve and index the regions (Fig. 5a). At the same time, an inter-pixel boundaries map $\Omega'_{w+1,h+1}$ is generated as shown in Fig. 5e.
- Step 2: According to the defined equations (6) - (13), the geometry (Fig. 5d) and the adjacency relations (Fig. 5a) are extracted for each region detected during the Step 1 by using both $\Omega'_{w+1,h+1}$ and the indexed image. Nodes, boundaries, borders are dynamically extracted from $\Omega'_{w+1,h+1}$ (Fig. 5c). The indexed image is used to retrieve neighbor's relations, carried by the boundary elements. Objects uniqueness has to be preserved and the extracted borders have to be oriented in the clockwise turn ($|CB|>0$). Both processes are controlled by the database D which ingest or not the proposed extracted objects (6) - (13). At this level, $\{N\}$, $\{B\}$, $\{CB\}$ are stored in D.
- Step 3: By analyzing topology relations (10) - (11), the regions are recursively created (14) and stored (15) in the tree structure (Fig. 5f.). Since every border CB_i is associated to a region R_i, starting from an image corner, region inclusions are recursively deduced and propagated to the whole segmented image by adjacencies relations.

The described algorithm allows building efficiently tree structures from segmented images without any parameters. It enables to deal directly with object oriented information. An order of computation time for the whole process on a standard PC (3 GHz, 1 Gb RAM) is 70 minutes for a 6144x6144 pixels RGB image.

5 DATA MERGING

DEM artifacts mainly lead to unrealistic views: In Fig. 3d, the lake should be a flat surface with an elevation lower than all its adjacent objects. The results achieved by object processing chain allow delimiting the 2D structure of the object to be regularized in the DEM. Registration errors between image and DEM are not taken into account. It remains to estimate the elevation surface of the object that depends on:

- DEM information,
- object shape and thematic, elevation modeling,
- neighboring relations

Thematics	Constraints and Modeling	
	Internal (border elevation H_{obj})	Neighbors (H_{neigh})
Sea, Lake, Canal	Horizontal surface	$H_{obj}<H_{neigh}$
Large building roof		$H_{obj}>H_{neigh}$
Airport, Parking, Football ground		-
Bridge, dam		$H_{obj}>H_{neigh}$
Street, Motorway	Tiled surface (small slope)	-
River		$H_{obj}<H_{neigh}$
Building, House	2 adjacent tiled surfaces (sym. slope)	$H_{obj}>H_{neigh}$
Forest	-	$H_{obj}>H_{neigh}$

Table I: Elevation constraints

Table I summarizes some of the objects which can be observed in RS images (medium to high resolution) and the constraints to be applied for the DEM regularization. Two types of constraints are modeled (internal / external). The first constraints are inferred by the object itself, whereas the others are related to the neighboring objects. In order to be able to apply these constraints on the DEM, the objects are labeled (e.g.

user interests, such as “forest”, “bridge”, “road”, etc.). To achieve the landscape recognition, an interactive object selection is achieved by the user as shown in Fig. 6b; it enables to link the regions to their user-defined cover types. Objects are selected through a Graphical User Interface (GUI) and classified according to their thematic coverage defined in Table I. The user’s “knowledge” as well as his specific interests is incorporated in a convenient way. From each studied thematic, a set of regions is extracted. Among them, adjacent or included regions are merged together by updating the tree structure. Interactively, the user refines the object selection until satisfactory cover type assignations are obtained.

The DEM regularization process is achieved in two stages; (i) to estimate the surface elevation, (ii) to control the transition, the shapes of the inserted objects. The object elevation models used are either horizontal or tiled (16) surfaces according to the defined thematic (Table I).

A least square problem is formulated to estimate the elevation surface of each object selected. DEM information are collected and classified in two categories (included H_{int} or excluded H_{ext} on the objects). Since elevation and image data may have different resolutions, the least square adjustment is applied on the DEM grid. Neighboring constraints are formulated through slope estimation $ds_{thematic\ j}$ for each adjacent thematic j between the interior and exterior observations (17). The elevation surface estimated is adjusted to respect the external constraints (Table I) carried by all the estimated $ds_{thematic\ j}$. Results are integrated in the DEM. The enhanced DEM is interpolated to match the image resolution. Finally, morphologic operators (dilation-erosion) are used to control the transitions and shapes in the border of the inserted objects, depending of the thematic of their adjacent objects.

$$X_i = (x_i, y_i, H_i),\ a\,x_i + b\,y_i + c\,H_i + d = 0 \tag{16}$$

$$ds_{thematic\ j} = \frac{H_{ext\ j} - H_{int}}{d_{ext-int}} \tag{17}$$

The enhancement obtained is presented in Fig. 6. Experiments have been done for tiled and horizontal surfaces such as “river”, “lake”, “airport”, “forest”, “sea”, “building” in a dataset composed of a SPOT 5 “Supermode” color image (resolution: 2.5m) and a X-band SRTM DEM (~22m). The object integration in the DEM is emphasized by Fig. 6. 3D rendering enhancements are presented in Fig. 6e and Fig. 6f, using respectively the filtered DEM and the regularized DEM. Thanks to the presented object line processing, significant improvements are achieved and more realistic 3D visualizations are obtained. Similarly, instead to estimate the surface of the objects, the integration of image-objects in the DEM can be realized to remove and clean the DEM from the contribution gathered by several thematic areas such as “forest”, “tree”, “building”, “car”, etc. This processing is determinant to optimally insert 3D synthetic objects coming from computer graphics or GIS databases.

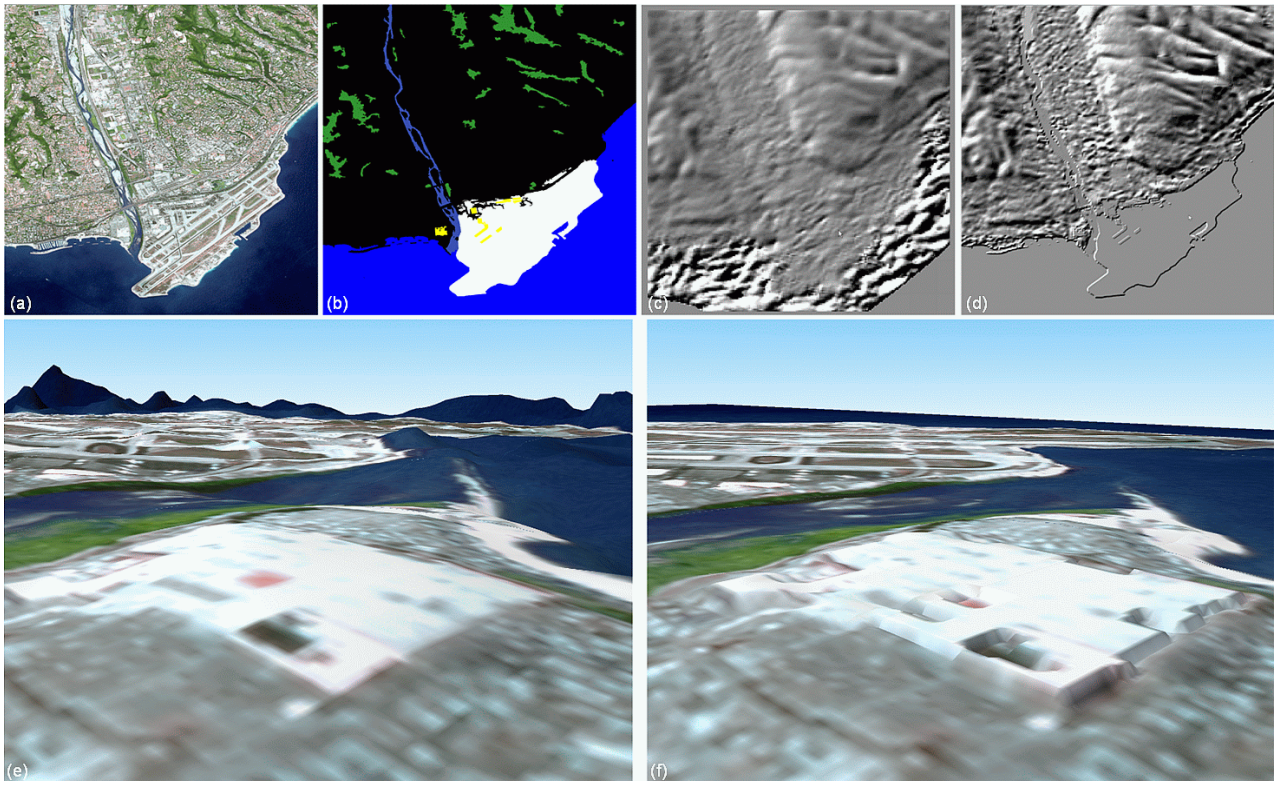

Fig. 6: Merging image-object in the DEM: Test site of Nice (France) with a SPOT5 “Supermode” image and X-SRTM DEM. (a) optical image, (b): user selection through GUI for the following thematic; *“large buildings” (yellow), “river” (dark blue), “sea” (light blue), “forest” (green), “airport” (white)*. (c)-(d): DEM improvements (slope visualization); (c) filtered DEM, (d) regularized DEM. (e)-(f): Perspective views with the filtered DEM (e) and with the regularized DEM (f).

6 CONCLUSION

Potential of SAR data to provide elevation data for ambitious and large virtual reality purposes is emphasized. To enhance and regularize the DEM data, a processing chain has been presented. These pre-processing steps are essential in order to generate a higher level of realism and to simplify the data for 3D rendering processes (meshes simplification, hierarchical decomposition, etc.). Such systems constitute a key step for realistic 3D visualizations of EO data. Thanks to the tree structure and the region growing algorithm, the processing line presented appears to be very efficient. The topology process does not require assumptions on the segmentation algorithm used. Topological and Geometric properties are directly encoded in the tree structure and provide coupled with the complex cellular approach a consistent and "natural" region description. The modeling of the tree structure and the information gathered by the topology analysis can be applied for other applications or fields such as pattern recognition, clustering, queries by content, etc.

REFERENCES

[1] P. Cignoni et al, "BDAM – Batched Dynamic Adaptive Meshes for High Performance Terrain Visualization*". Proc. EUROGRAPHICS'03*, vol 22 n°3: pp 505-514, 2003.

[2] C. Maire, M. Datcu, "EO and DEM information aggregation for realistic 3D visualization of natural landscapes*",* (submitted for publication). *IEEE Transactions on Geoscience and Remote Sensing,* submitted for publication.

[3] J.S. Lee, "Speckle suppression and analysis for synthetic aperture radar images", *Optical. Engineering*, vol. 25, n°5, pp 636-643, 1986.

[4] A Lopes, E. Nezry, R. Touzi, E. Nezry, "Structure detection and statistical adaptative speckle filtering in SAR images", *International Journal of Remote Sensing,* pp 1735-1758, 1993..

[5] D.L. Donoho, "De-noising by soft thresolding", *IEEE Transactions on Information Theory*, vol 41, n°3, pp 613-627, 1995.

[6] L.Gagnon, "Wavelet filtering of speckle noise. Some numerical results", *Conference Vision Interface'99,* 1999.

[7] C. Maire, M. Datcu, P. Audenino, "SAR DEM filtering by mean of Bayesian and multi-scale, nonstationary methods", *Proc IGARSS'03*, 2003.

[8] M. Walessa, M. Datcu, "Enhancement of interferometric DEMs by spatially adaptive model-based filtering in non-stationary noise"*, Proc. USAR2000*, pp 695-698, 2000.

[9] M. Datcu, K. Seidel, M. Walessa, "Spatial information retrieval from Remote Sensing Images: - Part I : Information theoretical perspectives", *IEEE Transactions on Geoscience. and Remote Sensing*, vol. 36, n°5 pp 1431-1445, 1998.

[10] N.R. Pal, S.K. Pal, "A review on image segmentation techniques", *Pattern Recognition*, vol. 26 n°9, pp 1277–1294, 1993.

[11] C. A. Bouman and M. Shapiro, "A multiscale random field model for Bayesian image segmentation", *IEEE Transactions on Image Processing*, vol. 3, n°2, pp 162–177, 1994.

[12] D. Comaniciu, P. Meer: Mean Shift: "A Robust Approach toward Feature Space Analysis", *IEEE Transactions Pattern Analysis and Machine Intelligence*, vol. 24, n°5, pp 603-619, 2002.

[13] G. Koepfler, C. Lopez, J. M. Morel, "A Multiscale Algorithm for Image Segmentation by Variational Method", *SIAM Journal on Numerical Analysis*, vol. 31 n°1, pp 282-299, 1994.

[14] Y.G. Leclerc, "Constructing simple stable descriptions for image partitioning", *Computer Vision*, vol. 3, pp 73-102, 1989.

[15] V.A. Kovalevsky, "Finite Topology as Applied to Image Analysis", *Computer Vision, Graphics, and Image Processing* n°46, pp 141-161, 1988.

[16] T.Y. Kong, A. Rosenfeld, "Digital Topology: Introduction and Survey", *Computer Vision, Graphics, and Image Processing* n°48, pp 357-393, 1989.

[17] C. Maire, M. Datcu, "Object and Topology extraction from Remote Sensing Images", *IEEE International Conference on Image Processing (ICIP) 2005*, Accepted paper, 2005.

[18] C. Maire, H. Yesou, "Storm forest damage mapping based on very high resolution data", *Proc FRINGE'03*, 2003.

[19] A. Koch, "An approach for the semantically correct integration of a Digital Terrain Model and a 2D GIS vector data set", *Proc ISPRS'04*, 2004.

[20] A. Carrara, G. Bitelli, R. Carla,. "Comparison of techniques for generating digital terrain models from contour lines", *International Journal of Geographical Information Science*, vol. 11, pp 451–473, 1997.

[21] T. Toutin, L. Gray, "State of the art of elevation extraction from satellite SAR data", *ISPRS Journal of Photogrammetry & RS*, vol. 55, pp 13-33, 1999.

[22] T. Toutin, "Elevation modeling from satellite visible and infrared (VIR) data: a review", *International Journal of Remote Sensing*, vol. 22, n°6, pp 1097-1125, 2001.

[23] R. Bamler, B. Schaettler, "SAR Data Acquisition and Image Formation", in *SAR geocoding: data and systems* G. Schreier (Ed.), Wichmann Verlag, Karlsruhe, pp. 53-102, 1993.